Journal of Applied Polymer Science

Encapsulated Phase Structure and Morphology Evolution During Quiescent Annealing in Ternary Polymer Blends with PA6 as Matrix

Rui Dou, Wei Wang, Yan Zhou, Lei Gong, Bo Yin, Ming-bo Yang

College of Polymer Science and Engineering, Sichuan University, State Key Laboratory of Polymer Materials Engineering, Chengdu 610065, Sichuan, China

Correspondence to: B. Yin (E-mail: yinbo@scu.edu.cn)

ABSTRACT: This work is aim to study the encapsulated morphology development in ternary blends of polyamide 6/high density polyethylene/maleic anhydride-*grafted*-ethylene propylene diene monomer (PA6/HDPE/EPDM-*g*-MA) and polyamide 6/maleic anhydride-*grafted*-high density polyethylene/ethylene propylene diene monomer (PA6/HDPE-*g*-MA/EPDM) through thermodynamically control described by Harkins spreading theory. The phase morphology was confirmed by using scanning electron microscope (SEM) and selective solvent extraction revealed that PA6/HDPE/EPDM-*g*-MA blend having a composition of 70/15/15 vol % is constituted of polyamide 6 matrix with dispersed composite droplets of HDPE subinclusions encapsulated by EPDM-*g*-MA phase, while for PA6/HDPE-*g*-MA/EPDM blend with the same composition is constituted of polyamide 6 matrix with dispersed composite droplets of HDPE-*g*-MA subinclusions encapsulated by EPDM phase. Quiescent annealing test revealed that for PA6/HDPE/EPDM-*g*-MA blend, a perfect core–shell structure with one HDPE particle encapsulated by EPDM-*g*-MA phase was formed during annealing, and for PA6/HDPE-*g*-MA/EPDM blend, a novel complete inverting HDPE-*g*-MA/EPDM core/shell structure was achieved. Moreover, quantitative analysis about coalescent behaviors of HDPE-*g*-MA and HDPE subinclusions during quiescent annealing were investigated by image analysis and the result suggested that the grafted maleic anhydride group in HDPE-*g*-MA, acted as a role of steric repulsion, could suppress coalescence effects, thus leaded to a lower coalescent rate than that of HDPE subinclusions. © 2013 Wiley Periodicals, Inc. J. Appl. Polym. Sci. **2014**, *131*, 39937.

KEYWORDS: blends; compatibilization; morphology; polyamides

Received 22 July 2013; accepted 8 September 2013

DOI: 10.1002/app.39937

INTRODUCTION

Ternary polymer blends have received extensive technological and academic interests over the last decade because of the possibility to obtain materials with combined properties of their components at a relatively low cost.[1–6] Generally speaking, the ultimate properties of polymer blends primarily depend on the phase morphology, which makes the control of phase morphology always a research focus. For an A/B/C ternary system in which A forms a continuous matrix, it is well known that two categories of morphologies exist: (1) materials B and C coexist as separate dispersed phases in the matrix; (2) core–shell droplets where one minor component encapsulates the other. With further subdivision, the core–shell morphology can also be divided into typical core-shell structure [Figure 1(a)] and multi-core dispersed phase morphologies [Figure 1(b, c)].

It should be pointed out that the final morphologies of polymer blends is a result of multiple factors including not only the thermodynamic factors, i.e., interfacial tension and surface free energy, but also the kinetic factors, i.e., viscoelastic properties and processing conditions. In most cases, interfacial tension effect, based on spreading theory, mainly determines the final phase morphologies of polymer blends. For ternary blends in which two minor components are mixed into the major one, the tendency for one phase to encapsulate a second one can be predicted by the following equation, which is an alternative form of Harkin's equation[7]:

$$\lambda_{CB} = \gamma_{BA} - \gamma_{CA} - \gamma_{BC} \quad (1)$$

where γ_{BA}, γ_{CA}, and γ_{BC} are the interfacial tensions for each component pair, and λ_{CB} is defined as the spreading coefficient for the shell forming component (C) on the core forming component (B). The index (A) refers to the matrix. A positive value of λ_{CB} indicates that phase (C) spreads over phase (B), leading to a separation of phases (A) and (B) by phase (C) at the interface. The use of this equation allowed a correct prediction of typical core–shell phase morphologies developed in the system

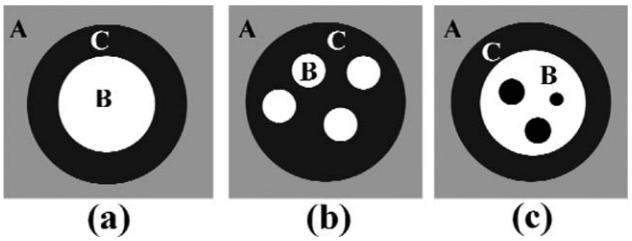

Figure 1. Schematic representation of morphologies of B/C composite droplets in a matrix A: (a) Encapsulated single particle of B in the shell of C; (b) Encapsulated multiple particles of B in the shell of C; (c) core–shell structure with shell subinclusions within the core.

of ternary blends such as high density polyethylene/polystyrene/polymethylmethacrylate (HDPE/PS/PMMA),[8–10] polypropylene/high density polyethylene/ethylene propylene diene monomer (PP/HDPE/EPDM),[11] polyamide 6/polypropylene/polystyrene (PA6/PP/PS),[12] and so on.

However, in some cases, the "multicore structure," i.e., several subinclusions of one minor phase are embedded in a larger particle of the second minor phase morphology cannot be successfully predicted by employing the spreading coefficient theory. Also, the morphology of subinclusions formation is related to various factors such as viscosity ratio,[13–16] elastic effect,[17,18] composition ratio effect,[19] interfacial reaction,[20,21] etc. Luzinov et al.[19] investigated the morphologies of ternary polystyrene/styrene–butadiene rubber/polyethylene (PS/SBR/PE) blends with a constant content of the major component (PS: 75 wt %), and found that according to the predication of spreading coefficients theory, the PE/SBR core–shell structure should be formed. However, in the melting process there exists a transformation from a multicore structure to PE/SBR core–shell morphology with different relative content of PE with respect to SER, corresponding to the theoretical composition of phase inversion for SBR/PE binary blends. Reignier and Favis[9] studied the effect of the component viscosity on the microstructure of HDPE/PS/PMMA ternary blends and found that the variation of the viscoelastic properties of the core in the dispersed phase dramatically affected PS-PMMA segregation within the dispersed composite droplet itself. A high-molecular-weight-PMMA core contained a large quantity of occluded PS inclusions, while the low-molecular-weight PMMA resulted in a perfectly segregated PS shell and PMMA core. Van Oene[17] showed that when the elasticity of the droplet exceeded that of the matrix, the free energy was always positive and was at a minimum when the number of inclusions inside the composite droplets equaled zero. Hence, no subinclusions appeared under these conditions. Also they presented experimental evidence that the formation of subinclusions resulted from the elasticity of the components and for any polymer pair, composite droplets can only be formed by the less elastic phase.

Our previous work was mainly focused on the formation of core–shell morphology in the PA6/HDPE/EPDM-*g*-MA blend. Li et al.[2] firstly discovered that the HDPE/EPDM-*g*-MA core/shell structure showed the outstanding superiority on the toughness improvement of PA6-based ternary blends compared to the rubber toughed PA6/EPDM blends. Also the difference of toughening mechanism between pure rubber particles in PA6/EPDM-*g*-MA binary blends and core–shell particles in PA6/EPDM-*g*-MA/HDPE ternary blends was clearly discussed. However, only one type of core–shell structure (encapsulated particle with EPDM-*g*-MA shell around one HDPE particle) was involved in the previous work. It is well known that the encapsulated morphology can be affected by many factors and can be displayed various microstructure such as multi-core structure (Figure 1).

The objective of this study is to examine the effect of two kinds of compatibilizers, HDPE-*g*-MA and EPDM-*g*-MA, on the encapsulated phase morphology of the two ternary blend systems of PA6/HDPE-*g*-MA/EPDM and PA6/HDPE/EPDM-*g*-MA with PA6 as the matrix. Furthermore, quiescent annealing was employed to investigate the microstructure equilibrium behavior in order to confirm the dominant effect of interfacial tension. Morphology evolution and coalescence behavior of subinclusions in the composite droplets was also quantificationally studied.

EXPERIMENTAL

Materials

Polyamide 6 (PA6), grade AKULON F136-C, was supplied by DSM, Netherland. HDPE 6098 and EPDM 4725P were from Qilu Petrochemical Company, China and Dow respectively. Maleic anhydride-*grafted*-ethylene-propylene-diene monomer (EPDM-*g*-MA), with the trademark Bondyram® 7003, was purchased from Polyram, Israel and maleic anhydride-*grafted*-high density polyethylene (HDPE-*g*-MA), with the trademark TRD-100H was from Yizheng Siruida Plastic Company, China. The properties of raw materials are listed in Table I.

Sample Preparation

PA6 was dried in a vacuum oven for 24 h at 80°C before blending to minimize the effects of moisture. Two ternary blending systems of PA6/HDPE/EPDM-*g*-MA and PA6/HDPE-*g*-MA/EPDM were prepared. All the blends were prepared by adding the raw materials simultaneously into the feed cylinder and melt blended using a co-rotating twin-screw extruder (Leistritz ZSE-18) with a screw diameter of 30.8 mm and an L/D ratio of 40. The screw speed was set at 150 rpm and a temperature profile of 230, 240, 250, 250, 250, 250, 250, 250, 250, and 245°C from the feeding zone to the die. After melt blending, the mixtures were quenched in cold water to freeze the morphology. The average shear rate was estimated to be $\gamma = 508.1\ s^{-1}$ based

Table I. Polymer Characteristics

Polymers	Density at 25°C (g/cm^3)	$\eta_0 \times 10^{-3}$ (Pa s) 250°C	Grafting degree (wt %)
PA6	1.13	2.0	-
HDPE	0.95	53.4	-
EPDM	0.88	14.2	-
HDPE-*g*-MA	0.93	15.0	1.5
EPDM-*g*-MA	0.88	9.7	0.7

Table II. Interfacial Tension for Polymer Pairs at 250°C

Polymer pairs	Interfacial tension (mN/m)
PA6/HDPE	22.1
PA6/EPDM-*g*-MA	0.9
EPDM-*g*-MA/HDPE	0.4
PA6/EPDM	22.6
PA6/HDPE-*g*-MA	0.7
EPDM/HDPE-*g*-MA	0.7

on the type of extruder. In this article, all the percentages given refer to volume percentages.

Interfacial Tension Measurement

Several methods can be used to evaluate the interfacial tension between molten polymers.[22] In our previous work, the interfacial tensions were calculated by Wu's equation.[23] However, it should be pointed that Wu's equation was improper to evaluate the interfacial tension for polymer pairs involving PA6 and maleic anhydride-*grafted*-copolymers (such as EPDM-*g*-MA and HDPE-*g*-MA in this article) due to the reaction between the carboxyl group in maleic anhydride of EPDM-*g*-MA or HDPE-*g*-MA and the amino end group of PA6. Therefore, the interfacial tension for the pairs of polymers in this study was determined using the rheological behavior of their respective blend. The data were analyzed using Gramespasher and Meissner's[24] analyses following the procedures reported elsewhere.[25–27] The results concerning the interfacial tensions are listed in Table II.

These interfacial tension data were used to calculate the spreading coefficients listed in Table III. For ternary blends of PA6/HDPE/EPDM-*g*-MA with PA6 as the matrix phase, it is predicted that HDPE particles should be completely engulfed by the EPDM-*g*-MA dispersed phase; while for PA6/HDPE-*g*-MA/EPDM with PA6 as the matrix phase, it is predicted that EPDM particles should be completely engulfed by the HDPE-*g*-MA dispersed phase.

Rheological Measurement

Rheological characterization was carried out using an AR2000ex stress controlled dynamic rheometer (TA Corporation) using a parallel plate geometry with 25 mm diameter at 250°C. In order to prevent thermo-oxidative degradation, all the tests were performed under nitrogen atmosphere. Disks of 25 mm diameter and 1.5 mm thickness were compression molded at 250°C, under a pressure of 10 MPa for 3 min. Time sweeps were performed at a frequency of 0.05 Hz and a constant strain of 2%.

Table III. Spreading Coefficients for the Ternary PA6/HDPE/EPDM-*g*-MA and PA6/HDPE-*g*-MA/EPDM Systems at 250°C

	Spreading coefficient (mN/m)
λ(EPDM-*g*-MA/HDPE)	20.8
λ(HDPE-*g*-MA/EPDM)	21.2

Steady-shear viscosity measurements of homopolymers were carried out using a RH7 high press capillary rheometer (Rohlin, England) under a temperature of 250°C in a shear rate range from 20 to 2000 s^{-1}.The measured shear viscosities of homopolymers are shown in Figure 2, and the viscosity ratio of HDPE/EPDM-*g*-MA and HDPE-*g*-MA/EPDM pairs is defined as the following equation:

$$\Psi = \eta_H / \eta_E \quad (2)$$

where Ψ represents the viscosity ratio, η_H represents the viscosity of HDPE or HDPE-*g*-MA, η_E represents the viscosity of EPDM or EPDM-*g*-MA, the calculated results are listed in Table IV.

Quiescent Annealing

Quiescent annealing was carried out in a compression molding press. Small pieces of samples were cut from the blend which were then sandwiched between two aluminum foil sheets and subsequently transferred into the cavity of a frame. The frame, together with the material, was then placed between two metal plates on the compression molding press. While annealing, the upper heating plate of the compression press just touched the metal plate on the sample without imposing any pressure in order to minimize any deformation or flow of the sample. The PA6/HDPE/EPDM-*g*-MA and PA6/HDPE-*g*-MA/EPDM blend was annealed at 250°C for three different duration time: 10, 30, and 60 min. After annealing, the samples were quenched immediately in liquid nitrogen to freeze the morphology.

Morphology Characterization

A JEOL JSM-5900LV scanning electron microscopy (SEM, JEOL, Japan) at a 20 kV accelerating voltage was used to observe the phase morphology of the blends. The samples were cryo-fractured in liquid nitrogen and the fractured surfaces were sputtered with gold before observation. In some cases, the cryogenically fractured surface was etched with xylene to remove the EPDM-*g*-MA or EPDM so as to strengthen the contrast between phases.

Quantitative analysis of the morphology was performed using image analysis of Image-Pro Plus 6. At least 300 dispersed domains were measured by manually tracing the phase boundaries to estimate number-average diameter (d_n) for each sample. Corrections to the particles size were performed using Schwartz–Saltykov method.[28]

RESULTS AND DISCUSSION

Morphologies of Binary and Ternary Blends

Figure 3(a,d) shows a typical morphology of the incompatible PA6/HDPE and PA6/EPDM blend, in which a dispersed droplet morphology and obvious interface were observed. Figure 3(b,e) gives SEM micrographs of PA6/EPDM-*g*-MA 70/30 and PA6/HDPE-*g*-MA 70/30 binary blends. It can be found the interface between two phases was very indistinct which means a good compatibility between PA6 and EPDM-*g*-MA or HDPE-*g*-MA. The reaction between the carboxyl group in maleic anhydride of EPDM-*g*-MA or HDPE-*g*-MA and the amino end group of PA6 tends to reduce the interfacial tension and prevent the aggregation of dispersed phase. Likewise, the SEM micrographs of PA6/HDPE/EPDM-*g*-MA and PA6/HDPE-*g*-MA/EPDM blends shown in Figure 3(c,f) indicate that the interface between dispersion

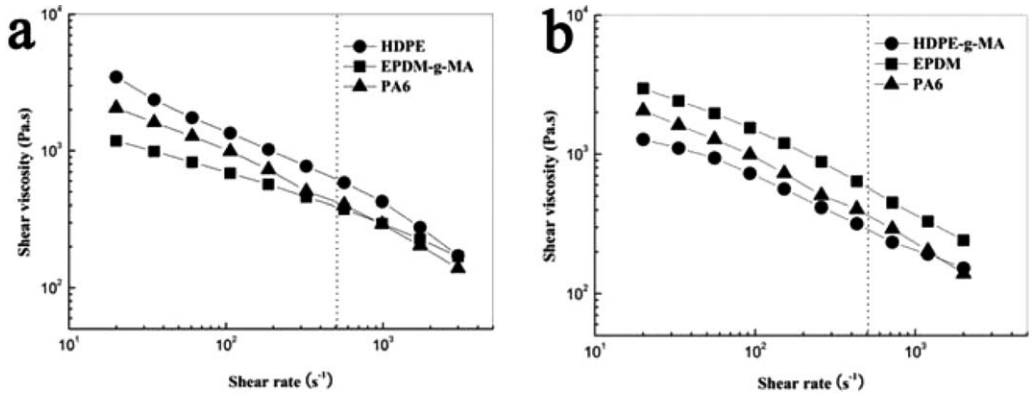

Figure 2. Shear viscosity as a function of shear rate at 250°C for PA6, HDPE, HDPE-*g*-MA, EPDM and EPDM-*g*-MA. The dashed lines represent the average shear rate during mixing.

phase and PA6 matrix becomes very obscure. It suggests that the three components strongly interact with each other, EPDM-*g*-MA and HDPE-*g*-MA compatibilizer has good compatibilization for the polymer pairs.

Morphologies of the Extruded Blends

Figure 4 shows the morphologies of PA6/HDPE/EPDM-*g*-MA and PA6/HDPE-*g*-MA/EPDM blends. By selective extraction of the EPDM or EPDM-*g*-MA phase, it is possible to create sufficient surface contrast to identify the phases. Subincluded HDPE particles embedded in the domain of EPDM-*g*-MA can be noticed after careful observation of morphologies of PA6/HDPE/EPDM-*g*-MA blends [Figure 4(a,c,e)]. Likewise, subincluded HDPE-*g*-MA particles embedded in the domain of EPDM can also be observed for PA6/HDPE-*g*-MA/EPDM blends [Figure 4(b,d,f)]. According to Luzinov et al.,[15] the transition to a core–shell structure is the result of an impeded phase-inversion phenomenon within the composite droplet itself. In order to clarify the reason for the formation of these morphologies, the following equation was used to predict the theoretical phase inversion, based on binary blends:

$$\eta_1/\eta_2 = \Phi_1/\Phi_2 \quad (3)$$

where η_1 and η_2 are the viscosities of the polymers at constant shear rate, corresponding to the processing conditions studied, and Φ_1 and Φ_2 are the volume fractions of polymers 1 and 2, respectively.

For binary blend of HDPE/EPDM-*g*-MA and HDPE-*g*-MA/EPDM, considering both eq. (3) and the viscosity of polymers, the calculated phase inversion volume fraction of HDPE and HDPE-*g*-MA is 61 and 34 vol %, respectively. As observed by Luzinov et al.,[15] the presence of subinclusions formation occurred at core (HDPE or HDPE-*g*-MA) contents much beyond that for phase inversion. Therefore, it is clear that the transition in the core–shell formation for PA6/HDPE/EPDM-*g*-MA blend is not a result of phase inversion, while for PA6/HDPE-*g*-MA/EPDM blend the observation from Figure 4 was consistent with the results of Luzinov et al.[15]

Table IV. Parameters Used from the Calculation of Shear Viscosity at a Shear Rate of 508.17 s^{-1}

Polymer pair	Viscosity ratio (Ψ)
HDPE/EPDM-*g*-MA	1.57
HDPE-*g*-MA/EPDM	0.51

For PA6/HDPE/EPDM-*g*-MA system, it is not a possible explanation for the formation of HDPE subinculstions by employing the results of Luzinov et al.,[15] since EPDM-*g*-MA demonstrates a clear tendency to encapsulate HDPE. It is likely that these HDPE subinclusions are formed in the the initial stages of blending and are subsequently immobilized by the highly viscous EPDM-*g*-MA phase. The immobilization of HDPE subinclusions in the composite droplets is also encouraged by the relatively low HDPE/EPDM-*g*-MA interfacial tension (Table II), this is also consist with the results obtained by Reignier and Favis.[9]

Because of the reaction between the carboxyl group in maleic anhydride and the amino end group of PA6, EPDM-*g*-MA and HDPE-*g*-MA will act as a compatibilizer to stabilize morphology and homogenize the droplet size in ternary blend. The number-average diameter (d_n) of the composite droplets in the PA6/HDPE/EPDM-*g*-MA and PA6/HDPE-*g*-MA/EPDM blend is plotted versus the EPDM-*g*-MA and HDPE-*g*-MA composition in Figure 5(a,b), respectively. Obviously, the composite droplets size decrease with the EPDM-*g*-MA or HDPE-*g*-MA content for each series of blends. Indeed, the diameter decreases from 0.62 to 0.28 μm, and from 0.89 to 0.56 μm for the EPDM-*g*-MA and HDPE-*g*-MA containing blends, respectively. This good compatibilizing effect of EPDM-*g*-MA and HDPE-*g*-MA induced a drastic decrease in interfacial tension and suppression of coalescence, leading to smaller droplets size. It is, however, worth noting that the droplets size in PA6/HDPE/EPDM-*g*-MA blend are less than that in PA6/HDPE-*g*-MA/EPDM with the same content of compatibilizer (EPDM-*g*-MA or HDPE-*g*-MA). This observation can be explained as follows. From Figure 4(e,f), it can be seen that nearly all HDPE-*g*-MA are located within EPDM phase for PA6/HDPE-*g*-MA/EPDM blend, while EPDM-*g*-MA phase prefers to forming a interfacial layer to encapsulate HDPE subinclusions for PA6/HDPE/EPDM-*g*-MA blend. Definately, the compatibilizer of EPDM-*g*-MA located at interface will play a much more remarkable compatibilizing effect during melt mixing, which

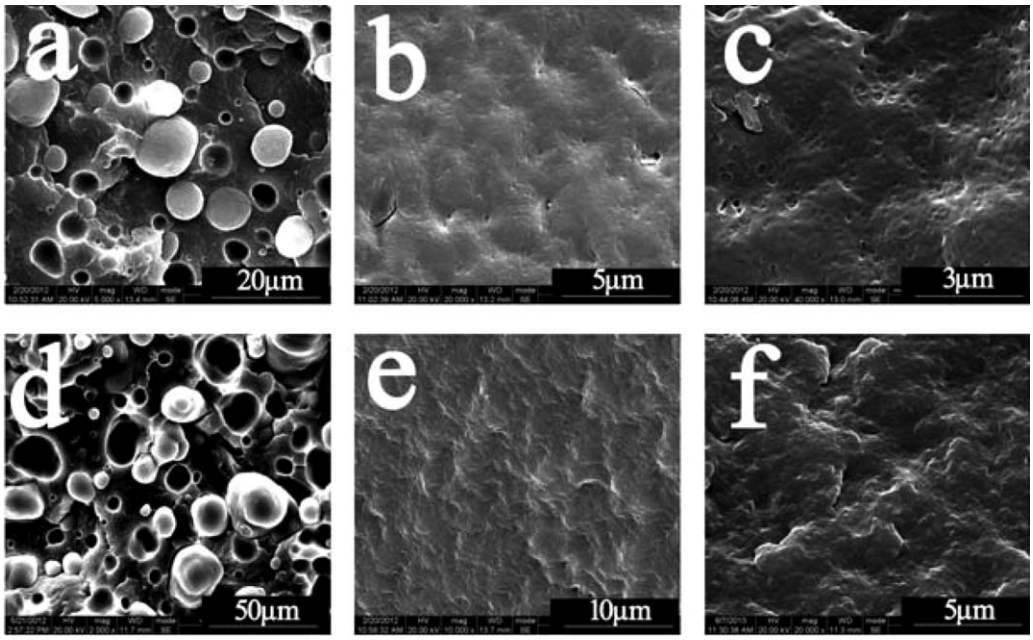

Figure 3. SEM micrographs of different polymer blends: (a) PA6/HDPE 70/30; (b) PA6/EPDM-*g*-MA 70/30; (c) PA6/HDPE/EPDM-*g*-MA 70/15/15; (d) PA6/EPDM 70/30; (e) PA6/HDPE-*g*-MA 70/30; (f) PA6/HDPE-*g*-MA/EPDM 70/15/15.

leads to a smaller droplets size in PA6/HDPE/EPDM-*g*-MA blend than that in HDPE-*g*-MA containing blends.

Morphology Evolution during Quiescent Annealing

In order to better investigate the microstructure equilibrium behavior and better visualize the blend structure, quiescent annealing was carried out. Quiescent annealing allows the interfacial forces dominate and leads the morphology to a thermodynamic steady state.

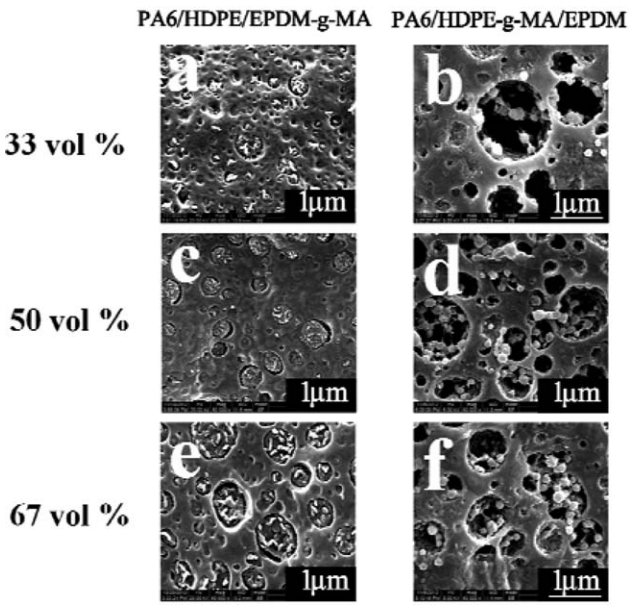

Figure 4. Morphologies of the blends as a function of the HDPE and HDPE-*g*-MA content(vol %, based on the dispersed phase) for the 70(PA6)/30(HDPE/EPDM-*g*-MA) blend (left column) and 70(PA6)/30(HDPE-*g*-MA/EPDM) blend (right column).

Figure 6 shows the morphology evolution of PA6/HDPE/EPDM-*g*-MA blend annealed at 250°C. The initial morphology observed in Figure 4(c) (0 min) shows a subinclusions of HDPE particles in the EPDM-*g*-MA phase. As the blend is annealed, HDPE subinclusions aggregate with increasing annealing time indicating that significant coarsening takes place. After 20 min of quiescent annealing, the HDPE phase has coalesced significantly at the core of the droplets before converting to an almost complete HDPE/EPDM-*g*-MA core/shell structure after 60 min [Figure 6(c)]. The morphology evolution of PA6/HDPE-*g*-MA/EPDM blend during annealing is shown in Figure 7. With annealing time increasing, HDPE-*g*-MA subinclusions tend to coarsen and migrate to the PA6/EPDM interface. After 20 min of quiescent annealing, most HDPE-*g*-MA phase has migrated to the PA6 matrix boundary before inverting to an almost complete HDPE-*g*-MA/EPDM shell/core structure (EPDM phase located within the HDPE-*g*-MA region) after 60 min [Figure 7(c)]. Undoubtedly, for PA6/HDPE-*g*-MA/EPDM blend, it can be believed that a perfect HDPE-*g*-MA/EPDM shell/core structure could be formed after sufficient time for quiescent annealing. The above analysis suggests that a core–shell structure consisting of HDPE core and EPDM-*g*-MA shell could be obtained in PA6/HDPE/EPDM-*g*-MA blend and a core–shell structure consisting of EPDM core and HDPE-*g*-MA shell could be obtained in PA6/HDPE-*g*-MA/EPDM blend, which are consistent with the results predicated by spreading coefficient (Table III).

It is well known that coalescence in molten polymer blend can often be observed during quiescent annealing.[29–33] For an uncompatibilized blend with sea-island morphology, the increase in droplets size with annealing time following the general power law[34]:

$$R^3(t) = R^3(0) + kt \quad (4)$$

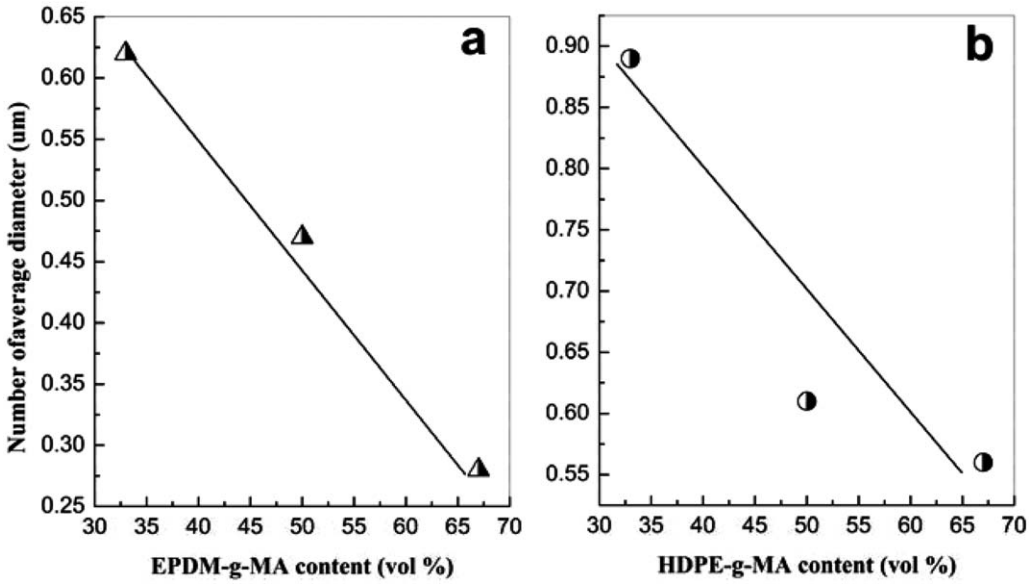

Figure 5. Effect of the (a) EPDM-*g*-MA and (b) HDPE-*g*-MA content (vol % based on the dispersed phae) on the number-average diameter of the composite droplets, for blend of PA6/HDPE/EPDM-*g*-MA and PA6/HDPE-*g*-MA/EPDM, respectively.

where R^3 is the cube of the average particle radius, R^3 (0) being the initial value at $t = 0$. The $t = 0$ is arbitrary, k is the coarsening constant, which depends on the mechanism, annealing temperature, volume fraction of the dispersed phase, etc. This equation reveals that R^3 increases linearly with time. For a compatibilized blend with sea-island morphology, the compatibilizer located at interface could effectively lower the interfacial tension and stabilize the morphology against coalescence.[35] The suppression of coalescence during annealing of compatibilized blend suggests that copolymers can prevent coalescence via steric stabilization.[36–39]

A quantitative analysis of the size of the dispersed droplets was carried out. The number average diameter (d_n) of composite droplets in PA6/HDPE/EPDM-*g*-MA and PA6/HDPE-*g*-MA/EPDM blend obtained using image analysis were plotted as a function of annealing time, as shown in Figure 8.

For PA6/HDPE/EPDM-*g*-MA blend, the size of the dispersed droplets is independent of the annealing time, meanwhile the particle d_n keeps almost a constant value of 0.47 μm. The main reason can be attributed to the reaction between the carboxyl group in maleic anhydride of EPDM-*g*-MA and the amino end group of PA6.[40] EPDM-*g*-MA phase, as an emulsifier, located at the PA6/HDPE interface would form a layer of EPDM-*g*-PA6 copolymer and effectively suppresses the coalescence of dispersed phase and stabilizes morphology.[41] In addition, the interfacial viscosity increases upon adding a compatibilizer (EPDM-*g*-MA), it will be difficult for the EPDM-*g*-PA6 copolymer to move. Thus, coalescence is greatly retarded during the annealing and the size of composite droplets in PA6/HDPE/EPDM-*g*-MA blend can remain stable for even an hour (Figure 8). However, quiescent annealing leads to a relatively significant reduction of the size of composite droplets for PA6/HDPE-*g*-MA/EPDM blends. Indeed, the calculated d_n of the initial composite droplets was 0.61 μm and the diameter decreases to 0.52 and 0.44 μm after annealing for 20 and 40 min, respectively, and finally to 0.42 μm after annealing for 60 min. Because of the existence of compatibilizer, i.e., HDPE-*g*-MA, it is obvious that both Ostwald ripening[41–43] and coalescence[44] mechanisms are not enough to understand the diameter decrease of composite droplets in the PA6/HDPE-*g*-MA/EPDM blend during annealing. From our understanding, it can be explained from the following reasons. On the one hand,

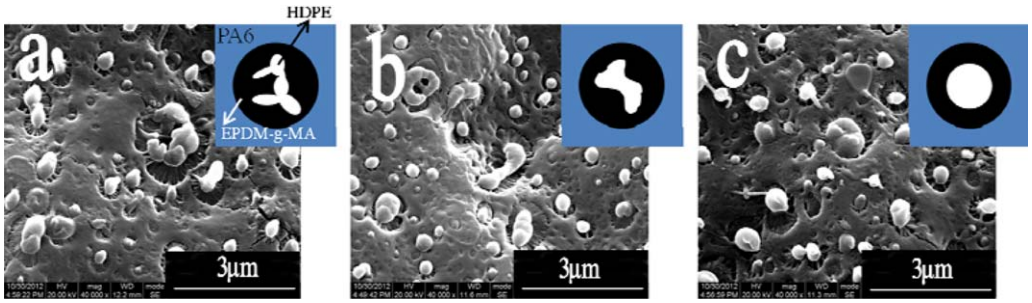

Figure 6. SEM micrograph of PA6/HDPE/EPDM-*g*-MA (70/15/15 vol %) blend after annealing for (a) 10 min, (b) 20 min, and (c) 60 min at 250°C. Note that the EPDM-*g*-MA has been extracted with xylene to enhance the contrast between the phases. [Color figure can be viewed in the online issue, which is available at wileyonlinelibrary.com.]

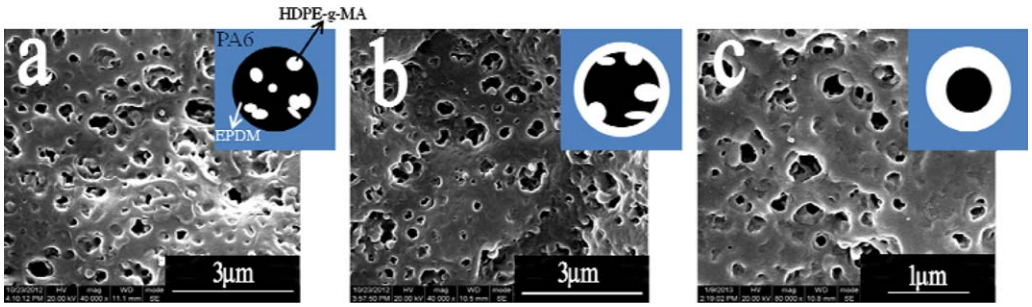

Figure 7. SEM micrograph of PA6/HDPE-*g*-MA /EPDM (70/15/15 vol %) blend after annealing for (a) 10 min, (b) 20 min, and (c) 60 min at 250°C. Note that the EPDM has been extracted with xylene to enhance the contrast between the phases. [Color figure can be viewed in the online issue, which is available at wileyonlinelibrary.com.]

the initial morphology of PA6/HDPE-*g*-MA/EPDM blend before annealing shown in Figure 4(d) shows that all the HDPE-*g*-MA subinclusions are located within the EPDM region rather than the PA6/EPDM interface, which weakens the ability of HDPE-*g*-MA to stabilize the phase morphology. On the other hand, based on the drive force of interfacial tension, HDPE-*g*-MA phase is apt to migrate to the PA6/EPDM interface and suppress the coalescence during annealing. Thus, the diameter decrease of composite droplets is likely caused by the reduction of the interfacial tension as well as the volume relaxation of dispersed phase during annealing above melting point. Moreover, the morphology evolution of PA6/HDPE/EPDM-*g*-MA and PA6/HDPE-*g*-MA/EPDM blends during annealing can also be reflected in the time sweep results as shown in Figure 9, which clearly show that the elastic modulus of the two blends rose with time, indirectly signifying the change of phase structures during annealing. However, the amplification of the storage modulus ($\Delta G'/G'_0$) for PA6/HDPE-*g*-MA/EPDM blend with a value of 6.3 is considerably larger than that of 0.6 for PA6/HDPE/EPDM-*g*-MA blend, which means more significant changes of phase structures of the samples happened during annealing. The time-dependent tan δ curve in Figure 9(b) also gives similar results. For PA6/HDPE/EPDM-*g*-MA blend, the tan δ value keeps unchanged with increasing time

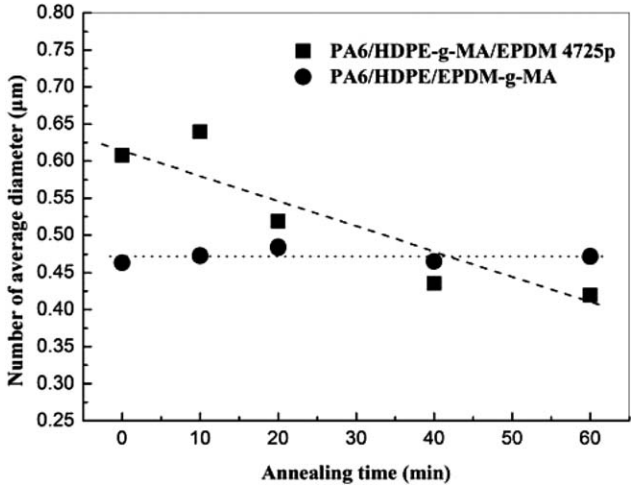

Figure 8. Effect of annealing time on the number average diameter (d_n) of composite droplets in PA6/HDPE-*g*-MA/EPDM and PA6/HDPE/EPDM-*g*-MA blend.

reflecting that the viscoelasticity of the blend melt barely changes, owning to the unchanged interfacial properties between phases during annealing shown in Figure 6, while for the PA6/HDPE-*g*-MA/EPDM blend, the tan δ increases with increasing time in the initial stage (time <17 min), and then monotonously decreases with increasing time from 17 to 120 min. The decline of tan δ means the elastic property of the blend melt becomes more significant, which is likely attributed to the changed interfacial properties induced by the formation of HDPE-*g*-PA6 copolymer when HDPE-*g*-MA migrates to the PA6/EPDM interface during annealing.

In order to further investigate the coalescent mechanism of subinclusions in composite droplets for PA6/HDPE/EPDM-*g*-MA and PA6/HDPE/EPDM-*g*-MA blend, we defined a parameter *K*, which means the average number of HDPE particles encapsulated in one EPDM-*g*-MA domain or the average number of HDPE-*g*-MA particles encapsulated in one EPDM domain. The value of *K* calculated from image analysis was drawn as a function of annealing time, and are shown in Figure 10. For PA6/HDPE-*g*-MA/EPDM blend, the value of *K* before annealing (annealing time = 0 min) is about 3.5 and with the annealing time increasing, *K* decreases from 2.7 to 2.0 when the annealing time increases from 10 to 40 min, afterwards to almost 1.0 after annealing for 60 min. However, for PA6/HDPE/EPDM-*g*-MA blend, unexpectedly, *K* dramatically decreases from 6.5 to 1.7 within the first 10 min annealing. With further annealing after 20 min, *K* keeps a constant value of nearly 1.0 even till annealing for 60 min. All in all, the curves shown in Figure 10 indicate that the coalescence mechanism of subincusions for the two blends display a significant difference.

Furthermore, we introduced parameter $1/t_{0.5K}$ to evaluate the coalescence rate of subinclusions (HDPE or HDPE-*g*-MA) in the composite droplets for both the two blends of PA6/HDPE-*g*-MA/EPDM and PA6/HDPE/EPDM-*g*-MA involved in our work, and $t_{0.5K}$ means the required annealing time that the value of *K* decrease to half of the initial value of *K*. The calculated $1/t_{0.5K}$ of different blends from Figure 10.

It can be found that for PA6/HDPE-*g*-MA/EPDM blend $1/t_{0.5K}$ has a value of 2.3×10^{-2} less than 14.5×10^{-2} for PA6/HDPE/EPDM-*g*-MA blend, which indicates HDPE-*g*-MA subinclusions in EPDM phase has a lower coalescence rate than that for HDPE subinclusions in EPDM-*g*-MA phase. The different

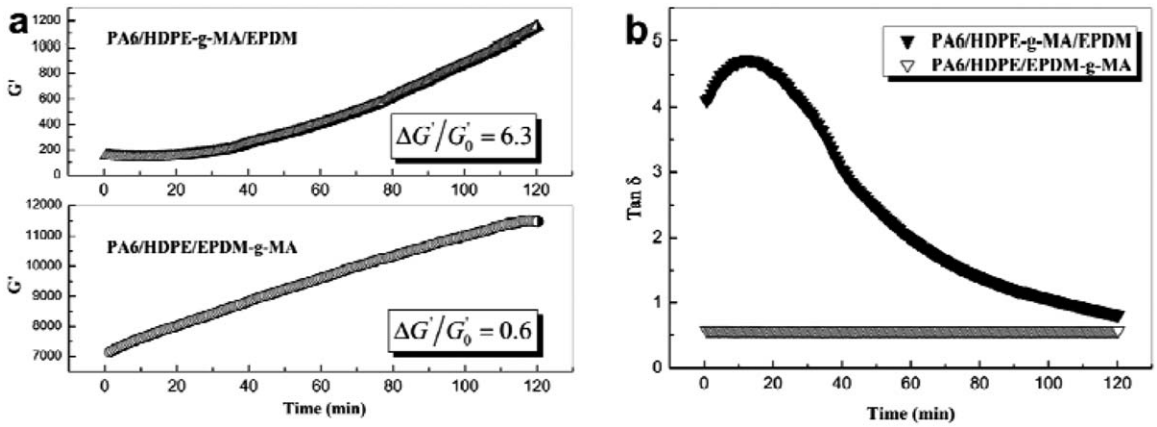

Figure 9. Time sweeps of the PA6/HDPE/EPDM-*g*-MA and PA6/HDPE-*g*-MA/EPDM blend at 0.05 Hz, 2% strain and 250°C: (a) storage modulus (G'); (b) loss tangent (tan δ). Here $\Delta G'/G'_0$ represents the ratio of the increment of storage modulus ($\Delta G'$) during time sweep to the initial storage modulus (G'_0) of the blend.

coalescence rate between HDPE-*g*-MA and HDPE is most probably caused by the different rheological properties of HDPE-*g*-MA/EPDM and HDPE/EPDM-*g*-MA pair. Generally speaking, coalescence during mixing will be governed by the interfacial mobility. The interfacial mobility of polymers described by van Gisbergen[45] shows that high polymer matrix viscosity should give rise to a relatively immobile interface which should result in long drainage times for the intervening film, consequently retard the coalescence. On the contrary, the rate of coalescence is expected to increase in the case of a less viscous matrix.[44] From Figure 2, it is obvious that EPDM has a higher viscosity than HDPE-*g*-MA for HDPE-*g*-MA/EPDM pair while EPDM-*g*-MA has a lower viscosity than HDPE for HDPE/EPDM-*g*-MA pair at the shear rate of 508.17 s^{-1}. Therefore, HDPE subinclusions should be merged more rapidly in a lower viscosity matrix of EPDM-*g*-MA for HDPE/EPDM-*g*-MA pair, as it is actually result. Moreover, there may be exists another probable reason responsible for the higher coalescence rate of HDPE subinclusions. It can be noted from Figures 8 and 10 that comparison with the PA6/HDPE-*g*-MA/EPDM blend, for the PA6/HDPE/EPDM-*g*-MA blend, the initial composite droplets diameter is smaller and the initial parameter K is larger, which means the average inter-HDPE subinclusion distance is shorter. This would enhance the contact opportunity of HDPE subinclusions, and in turns improves the coalescence rate of HDPE subinclusions. Likewise, it can be inferred that the grafted maleic anhydride group in HDPE-*g*-MA and the higher viscosity of EPDM cause the lower coalescence rate of HDPE-*g*-MA subinclusions.

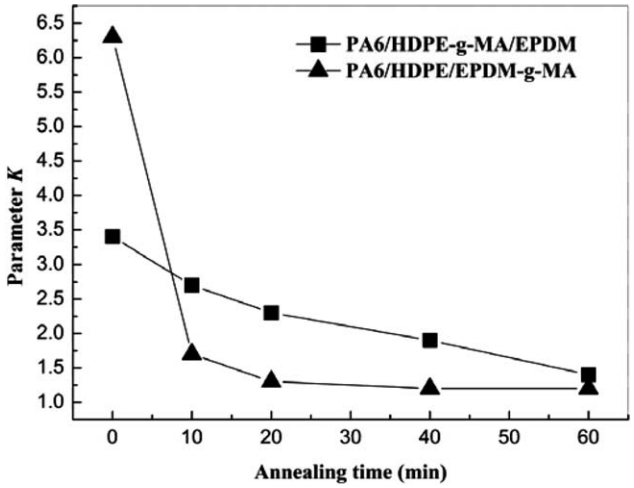

Figure 10. Effect of annealing time on the parameter K for PA6/HDPE-*g*-MA/EPDM and PA6/HDPE/EPDM-*g*-MA blend.

CONCLUSIONS

This study examines the issue of core–shell morphology formation and evolution for PA6/HDPE-*g*-MA/HDPE and PA6/HDPE/EPDM-*g*-MA systems. The initial phase morphology of PA6/HDPE-*g*-MA/EPDM and PA6/HDPE/EPDM-*g*-MA blend is observed as HDPE-*g*-MA suninclustions encapsulated by EPDM phase dispersed in PA6 matrix and HDPE subinclusions encapsulated by EPDM-*g*-MA phase dispersed in PA6 matrix, respectively. Quiescent annealing test results reveal HDPE-*g*-MA subinclusions tend to coarsening and migrate to the PA6/EPDM interface due to the drive of interfacial tension while HDPE subinclusions prefer to aggregate to a larger particle, which is consistent with the predication of spreading coefficient theory. In addition, the further investigated of coalescent behavior indicates that the coalescence rate of HDPE-*g*-MA subinclusions is lower than that of HDPE subinclusions which is caused by the steric hindrance effect of graft maleic anhydride group as well as the lower viscosity ratio of HDPE-*g*-MA/EPDM pair. Meanwhile, combining with the rheological measurement, different coalescent mechanism between the two blend systems is further revealed by employing time sweep.

ACKNOWLEDGMENTS

The authors gratefully acknowledge the financial support from the National Natural Science Foundation of China (Contract No. 51273219) and the National Key Basic Research Program of China (973 Program, No. 2012CB025902).

REFERENCES

1. Valera, T. S.; Morita, A. T.; Demarquette, N. R. *Macromolecules* **2006**, *39*, 2663.

2. Li, L. P.; Yin, B.; Zhou, Y.; Gong, L.; Yang, M. B.; Xie, B. H.; Chen, C. *Polymer* **2012**, *53*, 3043.
3. Ravati, S.; Favis, B. D. *Polymer* **2010**, *51*, 4547.
4. Corroller, P. L.; Favis, B. D. *Polymer* **2011**, *52*, 3827.
5. Majumdar, B.; Paul, D. R.; Oshinski, A. J. *Polymer* **1997**, *38*, 1787.
6. Galloway, J. A.; Macosko, C. W. *Polym. Eng. Sci.* **2004**, *44*, 714.
7. Hobbs, S. Y.; Dekkers, M. E. J.; Watkins, W. H. *J. Mater. Sci.* **1988**, *23*, 1598.
8. Reignier, J.; Favis, B. D. *Macromolecules* **2000**, *33*, 6998.
9. Reignier, J.; Favis, B. D. *AIChE J.* **2003**, *49*, 1014.
10. Guo, H. F.; Packirisamy, S.; Gvozdic, N. V.; Meier, D. J. *Polymer* **1997**, *38*, 785.
11. Li, L. P.; Yin, B.; Yang, M. B. *Polym. Eng. Sci.* **2011**, *51*, 2425.
12. Omonov, T.S.; Harrats, C.; Groeninckx, G. *Polymer* **2005**, *46*, 12322.
13. Gupta, A. K.; Srinivasan, K. R. *J. Appl. Polym. Sci.* **1993**, *47*, 167.
14. Nemirovski, N.; Siegmann, A.; Narkis, M. *J. Macromol. Sci. Part B: Phys.* **1995**, *34*, 459.
15. Luzinov, I.; Pagnoulle, C.; Jerome, R. *Polymer* **2000**, *41*, 7099.
16. Tchomakov, K. P.; Favis, B. D.; Huneault, M. A.; Champagne, M. F.; Tofan, F. *Polym. Eng. Sci.* **2004**, *44*, 749.
17. Vanoene, H. *J. Colloid Interface Sci.* **1972**, *40*, 448.
18. Legros, A.; Carreau, P. J.; Favis, B. D.; Michel, A. *Polymer* **1997**, *38*, 5085.
19. Luzinov, I.; Xi, K.; Pagnoulle, C.; Huynh-Ba, G.; Jérôme, R. *Polymer* **1999**, *40*, 2511.
20. Favis, B. D.; Lavallee, C.; Derdouri, A. *J. Mater. Sci.* **1992**, *27*, 4211.
21. Virgilio, N.; Sarazin, P.; Favis, B. D. *Polymer* **2011**, *52*, 1483.
22. Demarquette, N. R.; Souza, A. M. C.; Palmer, G.; Macaubas, P. H. P. *Polym. Eng. Sci.* **2003**, *43*, 670.
23. Wu, S. *Polymer Interface and Adhesion.* New York: Marcel Dekker, **1982**.
24. Gramespacher, H.; Meissner, J. *J. Rheol.* **1992**, *36*, 1127.
25. Souza, A. M. C.; Demarquette, N. R. *Polymer* **2002**, *43*, 1313.
26. Souza, A. M. C.; Demarquette, N. R. *Polymer* **2002**, *43*, 3959.
27. Macaubas, P. H. P.; Demarquette, N. R. *Polymer* **2001**, *42*, 2543.
28. Saltikov, S. A. *Proceedings of the Second International Congress for Stereology.* Springer-Verlag: New York, **1967**; pp 163–173.
29. Fortelny, I.; Kovár, J. *Polym. Compos.* **1988**, *9*, 119.
30. Cheng, T. W.; Keskkula, H.; Paul, D. R. *J. Appl. Polym. Sci.* **1992**, *45*, 1245.
31. Crist, B.; Nesarikar, A. R. *Macromolecules* **1995**, *28*, 890.
32. Fortelny, I.; Juza, J.; Dimzoski, B. *Eur. Polym. J.* **2012**, *48*, 1230.
33. Wallheinke, K.; Potschke, P.; Macosko, C. W.; Stutz, H. *Polym. Eng. Sci.* **1999**, *39*, 1022.
34. Zhu, L.; Yun, X.; Shen, X. Q.; Ding, W. X.; Zhao, H. Z.; Xu, X. H. *Colloid. Polym. Sci.* **2013**, *291*, 1669.
35. Sundararaj, U.; Macosko, C. W. *Macromolecules* **1995**, *28*, 2647.
36. Endo, S.; Min, K.; White, J. L.; Kyu, T. *Polym. Eng. Sci.* **1986**, *26*, 45.
37. Teyssie, P.; Fayt, R.; Jerome, R.; Makromol, C. *Macromol. Symp.* **1988**, *16*, 41.
38. Favis, B. D.; Chalifoux, J. P. *Polymer* **1988**, *29*, 1761.
39. Datta, S.; Lohse, D. J. *Macromolecules* **1993**, *26*, 2064.
40. Roeder, J.; Oliveira, R. V. B.; Goncalves, M. C.; Soldi, V.; Pires, A. T. N. *Polym. Test.* **2002**, *21*, 815.
41. Tadros, T. F.; Vincent, B. Emulsion stability. In: P Becher, ed *Encyclopedia of Emulsion Technology, Vol 1.* Marcel Dekker: New York, **1988**; Chapter 3.
42. Mirabella, F. M. *J. Polym. Sci. Part B: Polym. Phys.* **1994**, *32*, 1205.
43. Mirabella, F. M.; Barley, J. S. *J. Polym. Sci. Part B: Polym. Phys.* **1994**, *32*, 2187.
44. Fortelný, I.; Živný, A. *Polymer* **1988**, *39*, 2669.
45. van Gisbergen, J. G. M. Ph.D. Thesis. Eindhoven University of Technology, Eindhoven, The Netherlands, **1991**.